# Study of charged multiplicity distributions in $\bar{p}n$ interactions at 5.55, 9.3, and 14.6 GeV/$c$

A. Fridman, J.-P. Gerber, P. Juillot, A. Michalon, M.-E. Michalon-Mentzer, and C. Voltolini
*Centre de Recherches Nucléaires de Strasbourg, Strasbourg, France*

R. J. Plano and A. P. Sheng
*Rutgers—The State University, New Brunswick, New Jersey 08903*

E. B. Brucker, E. L. Koller, O. Raths, P. E. Stamer, and S. Taylor
*Stevens Institute of Technology, Hoboken, New Jersey 07030*

W. Hunt, J. A. Malko, and D. K. Robinson
*Case Western Reserve University, Cleveland, Ohio 44106*
(Received 3 June 1975)

We present a study of multiplicity distributions obtained from $\bar{p}n$ interactions based on three bubble chamber experiments carried out at Argonne (5.55 GeV/$c$), CERN (9.3 GeV/$c$), and Brookhaven (14.6 GeV/$c$). Only events having a visible track stopping in the chamber were used for the present analysis, thus allowing us to extract easily the coherent reactions from our data. The topological cross sections as well as various statistical moments obtained from the charged multiplicities are studied as functions of the incident momentum. Some comparison between our results and $\bar{p}p$ and $pp$ data is made.

## I. INTRODUCTION

We present here an analysis of charged multiplicity distributions at $\bar{p}$ incident momenta of 5.55, 9.3, and 14.6 GeV/$c$. The results were obtained from bubble chamber experiments carried out at Argonne (5.55 GeV/$c$), CERN (9.3 GeV/$c$), and Brookhaven (14.6 GeV/$c$). The data presented here are based on even-pronged events having a visible positive track stopping in the chamber.

At present little information exists on charged multiplicity distributions and topological cross sections for $\bar{p}n$ interactions. This is due primarily to the difficulty of extracting these quantities from the study of $\bar{p}d$ interactions. First of all, one has to note that the coherent production phenomena will complicate the analysis of the data. Indeed in coherent reactions the outgoing deuteron has a small laboratory momentum and can generally not be identified in the chamber unless kinematical fitting can be achieved. Therefore, we will extract the coherent reactions from our samples using the fact that these reactions present typical known kinematical configurations due to the form factor of the deuteron. In addition to the above difficulty, the determination of $\bar{p}n$ topological cross sections will be model dependent since we will assume an impulse approximation scheme for analyzing the $\bar{p}d$ interactions. Nevertheless, since the data at each momentum are treated in the same manner, they have the same type of systematic errors. Thus we have the possibility of studying the incident-momentum dependence of multiplicity distributions even if some uncertainty remains in the absolute values of the topological cross sections. In fact, the statistical moments calculated from the charged multiplicities are relatively independent of the systematic errors made in the calculations of the cross sections (see below).

In the next section we describe the experimental procedure as well as the problems arising in the cross section determination. Then we will discuss our data (Sec. III) and compare them with $\bar{p}p$ and $pp$ results. The conclusions of the present work are presented in Sec. IV.

## II. EXPERIMENTAL PROCEDURE

The film used for the present work was scanned for events having a visible positive track stopping in the bubble chamber. Events with an odd number of prongs were not taken because it is difficult to estimate for them the contribution of coherent reactions.[1] The drawback of this method is that one has to estimate the number of events having the momentum of the spectator proton $p_s$ below the threshold detection of the chamber, i.e., corresponding to a $p_s$ laboratory momentum of $p(p_s) \lesssim 0.1$ GeV/$c$.

For estimating the number of events, and consequently for calculating cross sections, we used the impulse approximation model assuming in particular that the spectator nucleon is not affected by the interaction. This picture is of course oversimplified as one neglects, among other things, screening effects, flux-factor corrections, the Pauli exclusion principle, and off-mass-shell corrections. These effects, in any case, appear to

have minor influence on the momentum distribution of the $p_s$ [2] which will serve us as the essential distribution for calculating the cross sections. The estimate of the events having invisible $p_s$ recoils depends on the expression chosen for the deuteron wave function although the most commonly used functions lead to similar $p_s$ momentum distributions in the $p(p_s) < 0.1$ GeV/$c$ region. This can be seen from Fig. 1 and also from Table I which gives the fraction of $p_s$ having their momentum in the $p(p_s) \lesssim 0.1$ GeV/$c$ range using different types of deuteron wave functions. For these cases one sees that the calculated fractions vary only within a few percent. However, for calculating cross sections we have to normalize our data in the $p(p_s) > 0.1$ GeV/$c$ region to the "theoretical" distribution calculated from the deuteron wave function. Then the obtained cross sections may vary in a rather important range according to the chosen deuteron wave function (last column of Table I).

In this work we will use throughout the Hulthén wave function. Apart from simplicity, this has the advantage of allowing comparisons of our data with other experiments since most of them are analyzed in terms of Hulthén distributions. In any case, in the framework of the impulse approximation the use of an approximate expression for the deuteron wave function can only introduce a systematic error which is incident momentum independent.

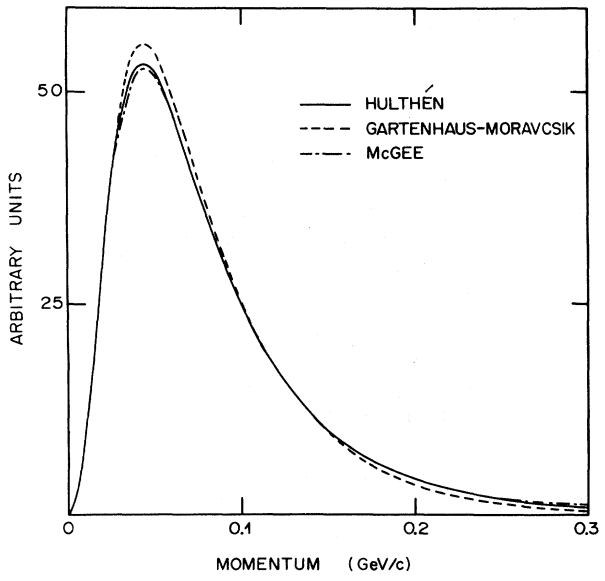


FIG. 1. Distributions of momenta of the nucleons inside the deuteron obtained from various deuteron wave functions. The dashed line is the curve obtained from the Gartenhaus-Moravcsik wave function. On the present scale no difference appears between the solutions II or III of the Gartenhaus-Moravcsik wave functions (see Table I and references quoted therein).

After these preliminary remarks we now describe in some detail the various steps used in determining the topological cross section $\sigma_n$, $n$ being the (odd) number of charged particles produced in the $\bar{p}n$ interactions. We first extract the coherent reactions from all the observed topologies. By coherent reactions we mean either reactions having an outgoing deuteron or reactions in which a $d^*$ enhancement appearing in the final state leads to $d^* \to d\pi$ or $d^* \to NN\pi$. We want to emphasize that the $d^* \to NN\pi$ phenomenon, which is usually interpretated as a $d\pi$ final-state interaction,[3,4] gives an important contribution to the $\bar{p}d$ production.[5] The rejection of these coherent events was made by studying the laboratory emission angle $\theta_s$ of the stopping track defined with respect to the incoming-beam direction. For real spectator events the $\cos\theta_s$ distribution has to be isotropic or a slightly increasing function of $\cos\theta_s$ if flux-factor corrections are important.[6] This situation is different for coherent reactions where the deuteron is emitted with a small laboratory momentum in the forward direction. As an example we present in Fig. 2 the $\cos\theta_s$ distribution for the four-pronged events at 5.55, 9.3, and 14.6 GeV/$c$ for which the coherent production is important. One notices the strong accumulation of events in the $\cos\theta_s \gtrsim 0.4$ region. By taking only the events located outside of these broad enhancements one obtains momentum distributions for the stopping track which are in good agreement with the Hulthén wave function predictions (full curves of Fig. 2). For the four-pronged events these will be the samples used in order to calcu-

TABLE I. Fraction of spectator protons having their laboratory momentum $p(p_s) < 0.1$ GeV/$c$ calculated with various deuteron wave functions (column 2). Column 3 gives the ratio $R$ between the cross sections calculated with the Hulthén wave function ($\sigma_H$) and the other type of functions ($\sigma_i$) whenever their resulting $p_s$ momentum distributions are normalized to our $p(p_s) > 0.1$ GeV/$c$ data.

| Wave function | Percentage | $R = \sigma_H/\sigma_i$ |
|---|---|---|
| Hulthén[a] | 80.61 | 1 |
| Gartenhaus-Moravcsik II[b] | 83.22 | 0.87 |
| Gartenhaus-Moravcsik III[b] | 83.06 | 0.87 |
| McGee[c] | 79.50 | 1.06 |

[a] L. Hulthén and M. Sugawara, *Handbuch der Physik*, edited by S. Flügge (Springer, Berlin, 1957).
[b] M. J. Moravcsik, Nucl. Phys. 7, 113 (1958).
[c] I. J. McGee, Phys. Rev. 151, 772 (1966).

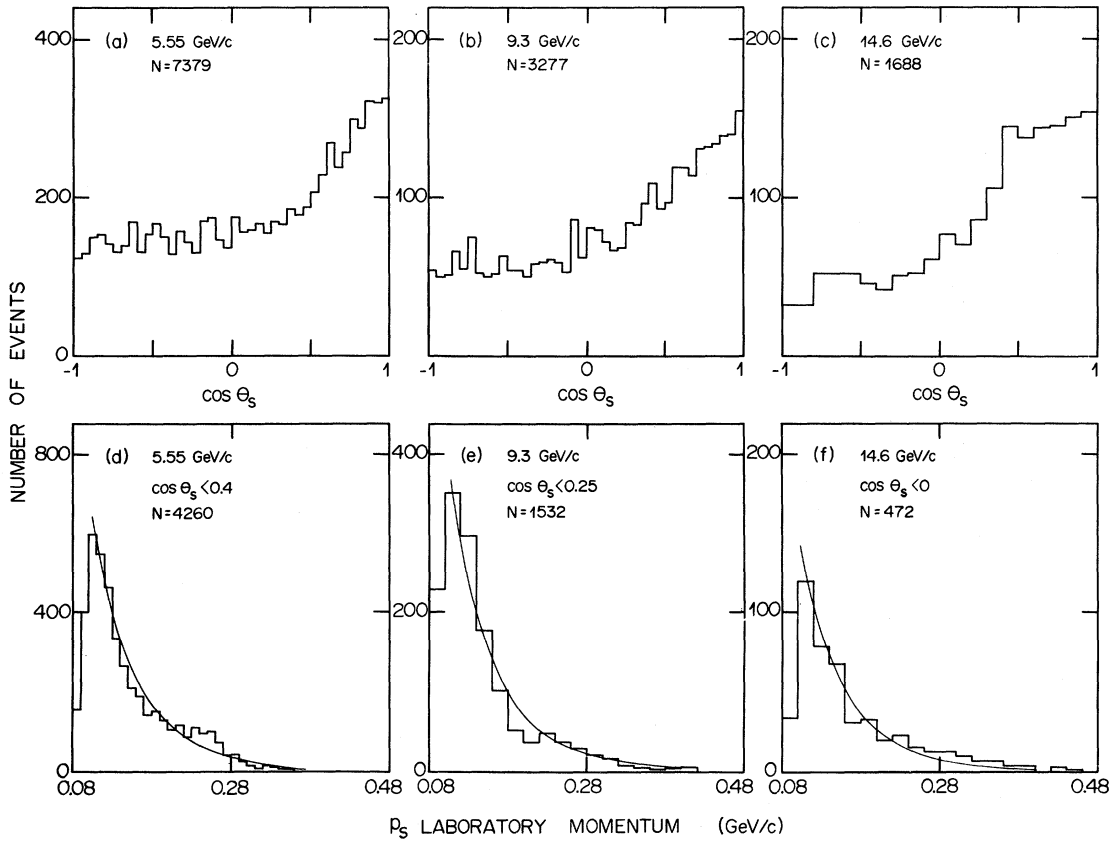


FIG. 2. The laboratory $\cos\theta_s$ distributions for the four-pronged events at (a) 5.55, (b) 9.3, and (c) 14.6 GeV/$c$ incident momenta, $\theta_s$ being the emission angle of the stopping outgoing track defined with respect to the incoming beam direction; (d), (e), and (f) show the laboratory momentum distribution of the stopping track for various $\cos\theta_s$ intervals. The full lines represent the Hulthén wave function predictions.

late the $\bar{p}n$ topological cross section $\sigma_n$. In order to illustrate in more detail the influence of coherent reactions on the $\cos\theta_s$ distribution we show in Fig. 3 various $\cos\theta_s$ distributions obtained from fitted channels at 5.55 GeV/$c$ where most of the exclusive reactions have already been studied.[5,7] Indeed, one observes the expected isotropic behavior for the events with $p_s$ in the final state [Fig. 3(a)], whereas the events having a deuteron are located in the $\cos\theta_s > 0.35$ region. For the $\bar{p}d \to \bar{p}\pi^- d^*$ channel where $d^* \to pn\pi$ one notices that the stopping track is emitted over a slightly broader $\cos\theta_s$ range.

Thus for each topology and at each of the three momenta we define a $\cos\theta_s$ range in which no coherent reactions are produced. The number of $\bar{p}n$ events thus lost are obtained by extrapolating each of the $\cos\theta_s$ distributions toward $\cos\theta_s = 1$ once the scanning corrections have been applied to our samples.

We distinguish essentially three sources of scanning losses which are (1) the losses due to events having stopping tracks that dip too steeply to be recorded or measured successfully; (2) the losses due to the scanning efficiency of the operators; (3) the losses introduced by the threshold detection ability of the bubble chamber.

The losses of type (1) were estimated by using the property of the stopping track to be isotropically distributed around the incident beam direction. A correction factor is then introduced to compensate for the observed lack of azimuthal symmetry due to undetected dipping stopping tracks. A further correction factor is calculated which takes into account the scanning efficiency of the operators [point (2)]. This latter correction is obtained from two separate scans of the film. Correcting the data for the various $\cos\theta_s$ cuts we finally estimate the number of events having their $p_s$ too short to be visible in the chamber [point (3)]. As stated above these numbers have been estimated by extrapolating the $p_s$ momentum distribution toward zero with the help of the Hulthén wave function. We used the parameter values of $\alpha = 0.046$

GeV/$c$ and $\beta = 0.260$ GeV/$c$ in the Hulthén wave function given in momentum space by:

$$\Phi(p) = \frac{1}{p^2+\alpha^2} - \frac{1}{p^2+\beta^2} ,$$

where $p$ denotes here the $p_s$ laboratory momentum.

By applying the corrections described above we obtained the topological cross sections for $n \geq 3$ given in Table II. We also give in this table the one-prong inelastic cross section $\sigma_1$ obtained by a subtraction procedure as will be explained in the next section. All the cross sections were calculated by taking into account the reduction of the incoming path length using the total $\bar{p}d$ cross sections $[\sigma_t(\bar{p}d)]$ given in Table III. No corrections for screening and double scattering were applied because of the difficulty of estimating such corrections for inelastic reactions. In any case, if one assumes that the percentage of screening and double scattering is independent of $n$, the estimated correction ($8\% \pm 3\%$) is nearly equal to the statistical errors on $\sigma_n$. Furthermore, the statistical moments are not very sensitive to the systematic errors made on $\sigma_n$ (see below).

### III. MULTIPLICITY DISTRIBUTIONS

Using our topological cross sections we present in Fig. 4 a comparison between $\bar{p}p$ and $\bar{p}n$ data in the 3–15 GeV/$c$ incident momentum region. For a given incident momentum one sees from this plot that, except for the three- and four-pronged events, $\sigma_n$ decreases with increasing $n$. Furthermore, one also notices the broadening of the $\bar{p}p$ and $\bar{p}n$ multiplicity distributions as the incident momentum $p_{\text{inc}}$ increases. For our results this is shown more clearly in Fig. 5 which presents $\sigma_n$ as a function of $n$ at each of our three momenta. For comparison we also put on this plot the $\sigma_n$ obtained from $\bar{p}p$ interactions using the available data at 5.7[8] and 14.75 GeV/$c$.[9] At 5.7 GeV/$c$ the $\bar{p}p$ data deviate rather strongly from the hand-drawn curve connecting our $\bar{p}n$ points. The situation is different at 14.75 GeV/$c$ where the $\sigma_n$ obtained from $\bar{p}p$ and

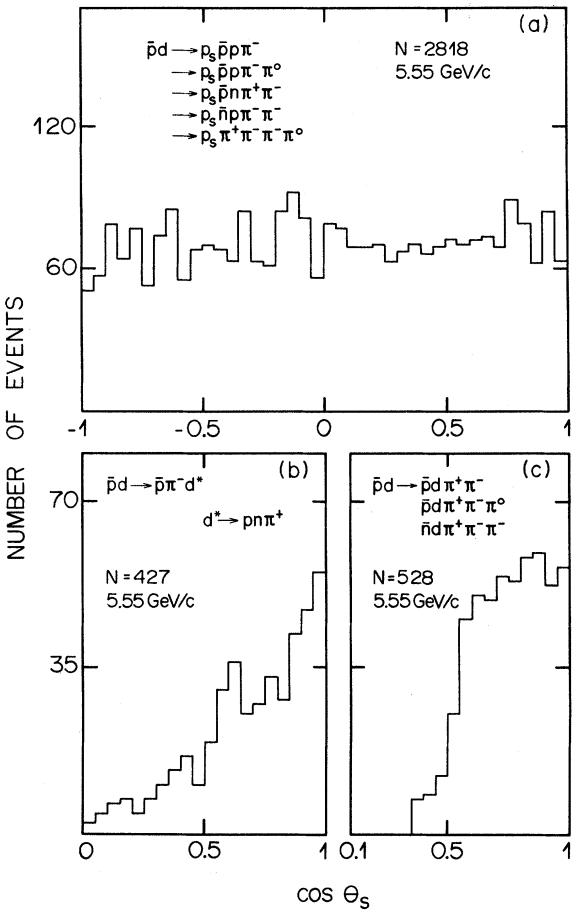


FIG. 3. The cos$\theta_s$ distribution for exclusive channels at 5.55 GeV/$c$ for (a) spectator events and (b), (c) for coherent reactions. Here $\theta_s$ is the emission angle of the stopping track defined with respect to the incident beam momentum.

$\bar{p}n$ interactions tend to be distributed on the same are interleaved.

Similarly to other high-energy reactions the average $\bar{p}n$ charged multiplicity $\langle n \rangle$ increases with $p_{\text{inc}}$. This is shown in Fig. 6 (see also Table IV) which compares the distribution of $\langle n \rangle$ as a func-

TABLE II. Topological $\bar{p}n$ cross sections (mb) obtained at 5.55, 9.3, and 14.6 GeV/$c$. The one-prong events ($n = 1$) were calculated as described in the text.

| Topology | Incident laboratory momentum (GeV/$c$) 5.55 | 9.3 | 14.6 |
|---|---|---|---|
| 1 | 13.1 ±4.0 | 12.4 ±2.8 | 9.1 ±1.8 |
| 3 | 14.05 ±0.77 | 13.69±0.95 | 13.8 ±1.1 |
| 5 | 8.93 ±0.67 | 8.43±0.81 | 10.8 ±0.9 |
| 7 | 2.21 ±0.18 | 4.36±0.53 | 5.3 ±0.5 |
| 9 | 0.24 ±0.03 | 1.04±0.19 | 1.7 ±0.2 |
| 11 | 0.018±0.004 | 0.13±0.03 | 0.28±0.03 |
| 13 | ≤0.002 | $(0.9 \pm 0.2) \times 10^{-2}$ | 0.05±0.01 |

TABLE III. Quantities (mb) used in calculating the multiplicity distributions. The total $\bar{p}d$ cross section $[\sigma_t(\bar{p}d)]$ was utilized for calculating the path length attenuation in the chamber. The $\bar{p}n$ elastic $[\sigma_{el}(\bar{p}n)]$ and total $[\sigma_t(\bar{p}n)]$ cross sections allowed us to calculate $\sigma_{in}=\sigma_t(\bar{p}n)-\sigma_{el}(\bar{p}n)$ and hence, $\sigma_1=\sigma_{in}-\sum_{n=3}\sigma_n$. Because of the lack of $\bar{p}n$ data $\sigma_{el}$ and $\sigma_t$ at 9.3 and 14.6 GeV/$c$ were taken from $\bar{p}p$ interactions.

| Cross section (mb) | Incident momentum (GeV/$c$) 5.55 | 9.3 | 14.6 |
|---|---|---|---|
| $\sigma_t(\bar{p}d)$ | $109.5\pm1.5$[a] | $100.6\pm1.8$[a] | $94.5\pm2.1$[a] |
| $\sigma_t(\bar{p}n)$ | $55\pm3$[b] | $52.9\pm2.4$[c] | $50.7\pm0.9$[d] |
| $\sigma_{el}(\bar{p}n)$ | $16.5\pm2.4$[b] | $12.8\pm0.6$[c] | $9.7\pm0.4$[d] |
| $\sigma_{in}(\bar{p}n)$ | $38.5\pm3.8$ | $40.1\pm2.5$ | $41.0\pm1.0$ |

[a] Interpolation from counter data (see Ref. 8).
[b] Reference 10.
[c] Values interpolated from the available $\bar{p}p$ data and taken from Ref. 8.
[d] $\bar{p}p$ values at 14.75 GeV (Ref. 9).

tion of $p_{inc}$ for $\bar{p}p$, $\bar{p}n$, and $pp$ interactions. One sees from this figure that our values are between those obtained from the $pp$ and $\bar{p}p$ data points. In fact for a given incident momentum our $\langle n\rangle$ values do not deviate very much from the $\bar{p}p$ results.

To calculate $\langle n\rangle$ for our results as well as the other statistical moments deduced from the $\bar{p}n$ charged multiplicities (Table IV) we have to know the one-prong inelastic cross section which cannot

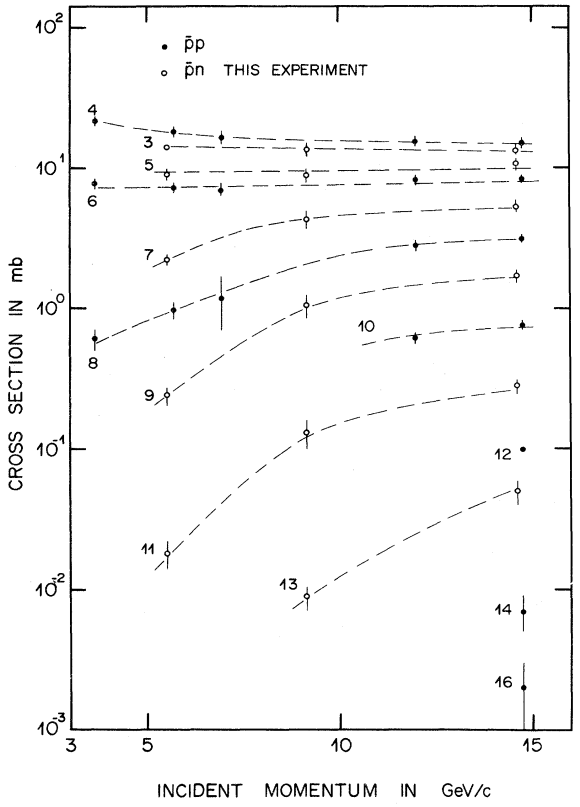


FIG. 4. Comparison between $\bar{p}p$ and $\bar{p}n$ topological cross sections in the 3–15 GeV/$c$ incident momentum region. The dashed lines are drawn to guide the eye.

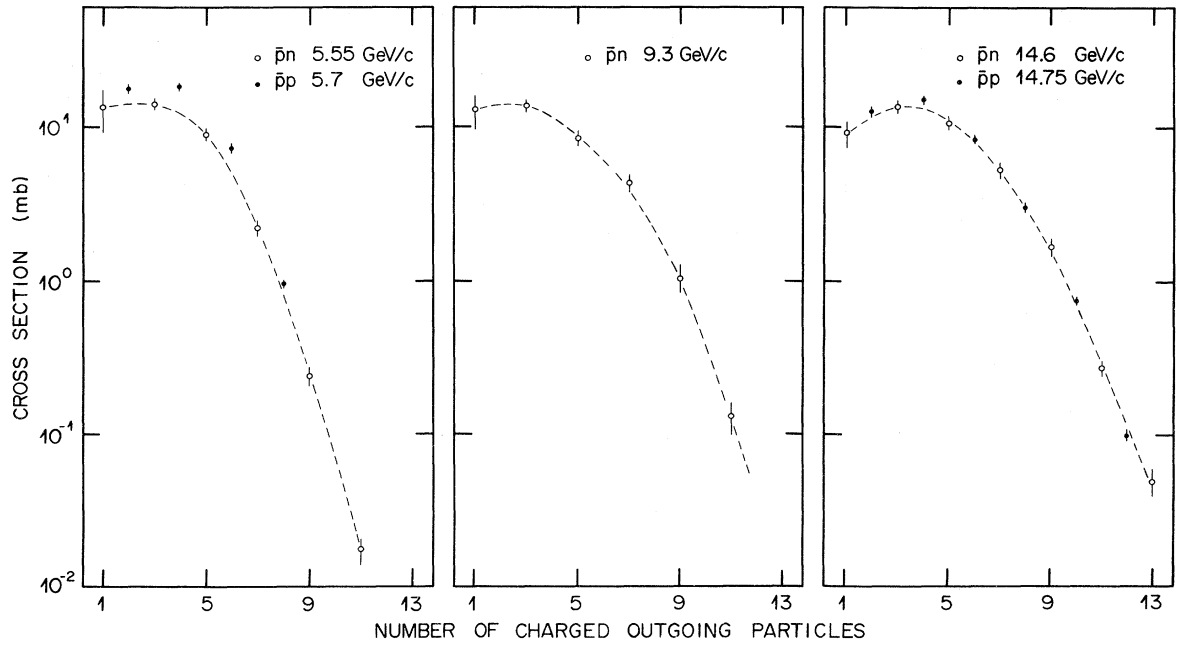


FIG. 5. Comparison of the $\bar{p}n$ topological cross sections plotted versus the number of charged outgoing particles with the available $\bar{p}p$ data. Note that the one-pronged $\bar{p}n$ cross section is calculated from the relation $\sigma_1=\sigma_t(\bar{p}n)-\sigma_{el}(\bar{p}n)-\sum_{n=3}\sigma_n$ (see text). The lines are drawn to guide the eye.

be easily determined from the study of $\bar{p}d$ interactions. Among other things this is because of the presence of the breakup $\bar{p}d \to \bar{p}pn$ reaction to which the spectator scheme cannot be applied.[10] Therefore we estimate $\sigma_1$ from the relation

$$\sigma_1 = \sigma_t(\bar{p}n) - \sigma_{el}(\bar{p}n) - \sum_{n=3} \sigma_n ,$$

where $\sigma_t(ab)$ and $\sigma_{el}(ab)$ are the total and elastic $a$-$b$ cross section, respectively. At 5.55 GeV/$c$ we use the values given in Ref. 10. At 9.3 and 14.6 GeV/$c$, for which there is no available $\bar{p}n$ data, we simply took $\sigma_t(\bar{p}n) = \sigma_t(\bar{p}p)$ and $\sigma_{el}(\bar{p}n) = \sigma_{el}(\bar{p}p)$ (see Table III) allowing us to obtain estimates of $\sigma_1$. Using these calculated values of $\sigma_1$ and our topological cross sections we have calculated the average of any given quantity $F$ from the relation

$$\langle F \rangle = \sum_{n=1} F \frac{\sigma_n}{\sigma_{in}} ,$$

the inelastic cross sections $\sigma_{in}$ being defined as

$$\sigma_{in} = \sigma_t(\bar{p}n) - \sigma_{el}(\bar{p}n)$$

and given in Table III.

The errors on $\sigma_1$ as well as those calculated for the moments given in Table IV were determined by a Monte Carlo method. We assumed that all the input quantities used to calculate $\sigma_1$ and any moment are distributed according to Gaussian distributions with widths given by the errors associated with the input quantities. The same procedure was applied to determine the errors on the quantities obtained from $\bar{p}p$ and $pp$ data in order to carry out the comparison with our results.

Although the errors are significant (due mainly to our method of calculating $\sigma_1$) some conclusions can be drawn by inspecting Table IV. It should be noted that the quantities calculated in Table IV are not too sensitive to the systematic errors which

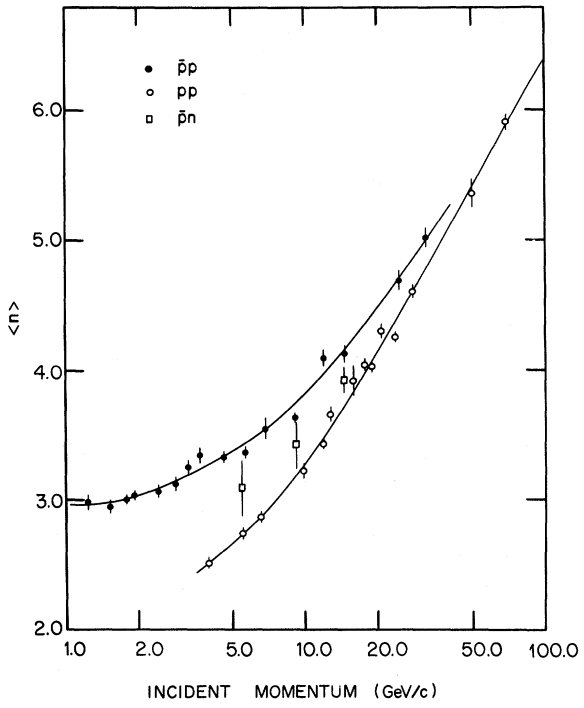


FIG. 6. Comparison between the average multiplicity for $pp$, $\bar{p}p$, and $\bar{p}n$ interactions as a function of the incident momentum. The full curves are drawn to guide the eye.

can be made in calculating the $\sigma_n$. Indeed by changing all the measured $\sigma_n$ by ±5% we still obtain values (Table V) which are compatible, within errors, with those given in Table IV. We first notice from this latter table that $D$, the dispersion of the charged multiplicity, and $f_2 = D^e - \langle n \rangle$ increase with $\langle n \rangle$ or equivalently with $p_{inc}$. Our $D$ values plotted as a function of $\langle n \rangle$ are compared with $\bar{p}p$ data in Fig. 7. We observe that for a given $\langle n \rangle$ the dispersion of the $\bar{p}n$ charged multiplicity is larger

TABLE IV. Statistical moments calculated from the charged multiplicities obtained in $\bar{p}n$ interactions at 5.55, 9.3, and 14.6 GeV/$c$.

| | 5.55 GeV/$c$ | 9.3 GeV/$c$ | 14.6 GeV/$c$ |
|---|---|---|---|
| $\langle n \rangle$ | 3.09 ± 0.23 | 3.43 ± 0.19 | 3.92 ± 0.10 |
| $c_2 = \langle n^2 \rangle / \langle n \rangle^2$ | 1.36 ± 0.06 | 1.41 ± 0.05 | 1.34 ± 0.02 |
| $c_3 = \langle n^3 \rangle / \langle n \rangle^3$ | 2.23 ± 0.25 | 2.42 ± 0.21 | 2.14 ± 0.09 |
| $c_4 = \langle n^4 \rangle / \langle n \rangle^4$ | 4.11 ± 0.74 | 4.72 ± 0.66 | 3.88 ± 0.25 |
| $D = [\langle n^2 \rangle - \langle n \rangle^2]^{1/2}$ | 1.84 ± 0.05 | 2.18 ± 0.05 | 2.28 ± 0.05 |
| $\langle n \rangle / D$ | 1.68 ± 0.16 | 1.57 ± 0.10 | 1.72 ± 0.06 |
| $f_2 = D^2 - \langle n \rangle$ | 0.30 ± 0.37 | 1.34 ± 0.32 | 1.30 ± 0.25 |

TABLE V. Range of the statistical moments calculated from the charged multiplicities when all the measured topological cross sections are varied by ±5%. Note that the values found are compatible within errors with those given in Table IV.

| | 5.55 GeV/$c$ −5% +5% | 9.3 GeV/$c$ −5% +5% | 14.6 GeV/$c$ −5% +5% |
|---|---|---|---|
| $\langle n\rangle$ | 2.98–3.19 | 3.31–3.55 | 3.77–4.06 |
| $c_2$ | 1.39–1.34 | 1.44–1.38 | 1.38–1.31 |
| $c_3$ | 2.35–2.12 | 2.57–2.30 | 2.29–2.02 |
| $c_4$ | 4.49–3.79 | 5.22–4.35 | 4.31–3.53 |
| $D$ | 1.85–1.82 | 2.19–2.17 | 2.31–2.24 |
| $\langle n\rangle/D$ | 1.61–1.75 | 1.51–1.64 | 1.63–1.82 |
| $f_2$ | 0.45–0.14 | 1.51–1.16 | 1.57–0.95 |

than the $\bar{p}p$ one. In other words it appears that for a fixed $p_{\text{inc}}$ value the disperions $D$ is greater for $\bar{p}n$ than for $\bar{p}p$ in contrast to the average charged multiplicities. Using Table IV we also see that the $c_q = \langle n^q\rangle/\langle n\rangle^q$ ($q = 1, 4$) and $\langle n\rangle/D$ ratios are not very dependent on $p_{\text{inc}}$ as expected if the data were to fulfil the early Koba-Nielson-Olesen (KNO) scaling.[11] In fact by plotting our data in the form of $\langle n\rangle\sigma_n/\sigma_{\text{in}}$ versus $n/\langle n\rangle$ (Fig. 8) it appears that our points tend to be distributed on a curve which is, however, different from the one obtained by fitting either the $pp$[12] (full curve) or the $\bar{p}p$[13] (dashed curve) data. As can be seen from Fig. 8 our points deviate rather strongly from the fitted $pp$ and $\bar{p}p$ curves, especially for high multiplicities.

This discrepancy can be understood if, following a suggestion made by Berger,[14] one considers the apparent KNO scaling as a consequence of the so-called empirical Wroblewski-Malhotra rule.[15,16] This rule relates the dispersion of the charged multiplicity with its average through the linear expression

$$D = c\langle n\rangle - c'$$

leading to approximate constancy of $D/\langle n\rangle$ for high-energy reactions. Here $c$ and $c'$ are parameters which, for $pp$ interactions, are found to be (Ref. 15)

$$c = c' = 0.58 \pm 0.01 .$$

Thus in the limit where for a given type of interaction particle $D/\langle n\rangle$ is approximately constant (i.e., independent of the c.m. energy) one can understand the apparent scaling behavior shown by the data. Indeed the distributions $\langle n\rangle\sigma_n/\sigma_{\text{in}}$ plotted versus $n/\langle n\rangle$ are all normalized to nearly one (this would be strictly true if the probability $\sigma_n/\sigma_{\text{in}}$ would be a continuous function of $n$) while the $n/\langle n\rangle$ variable has an average of one and nearly the same dispersion $D/\langle n\rangle$. It may then be con-

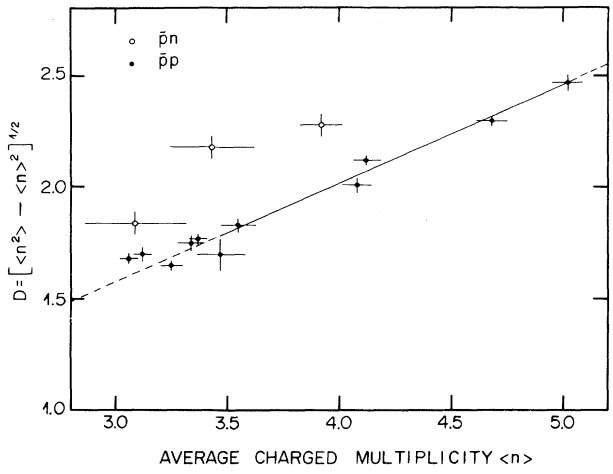


FIG. 7. The dispersion $D$ of the charged multiplicity versus its average $\langle n\rangle$ for our results and the $\bar{p}p$ interactions. By fitting the straight line to the $\bar{p}p$ data in the $\langle n\rangle > 3.5$ region we only took into account the errors on the $D$ quantities.

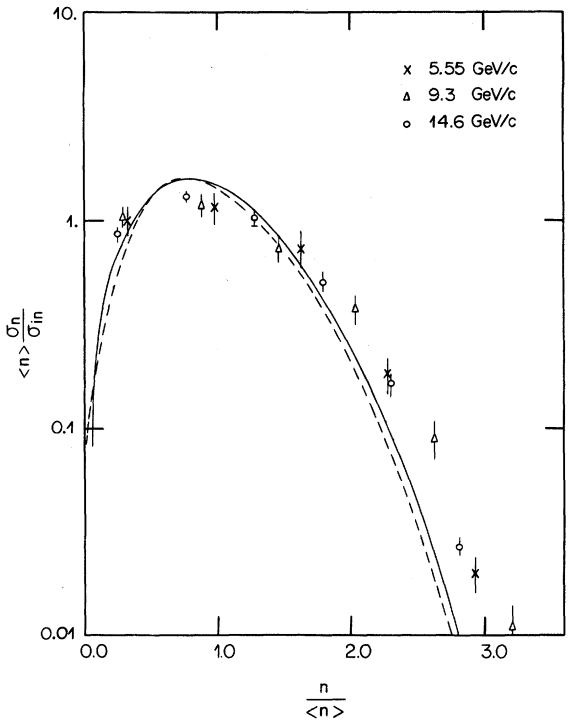


FIG. 8. The distribution of $\langle n\rangle\sigma_n/\sigma_{\text{in}}$ versus $n/\langle n\rangle$ for the $\bar{p}n$ interactions at 5.55, 9.3, and 14.6 GeV/$c$. The full and dashed line are obtained by fitting the $pp$ and $\bar{p}p$ data (see text).

ceivable that the distribution of $\langle n\rangle\sigma_n/\sigma_{in}$ versus $n/\langle n\rangle$ present a scaling behavior for a given type of incoming particle. In fact by fitting the $D = c\langle n\rangle - c'$ function to the $\bar{p}p$ data (see Fig. 7) in the range of $\langle n\rangle > 3.5$, corresponding to $p_{inc} > 6.9$ GeV/$c$, one obtains:

$$c = 0.44 \pm 0.02 ,$$

$$c' = -0.54 \pm 0.25 .$$

These values are different from those obtained for $pp$ interactions. For the $\bar{p}n$ case we do not have enough data points to carry out a meaningful fit. In any case in the approach discussed in Ref. 14 the different values of the $D/\langle n\rangle$ ratio may explain the difference observed between the $pp$, $\bar{p}p$, and $\bar{p}n$ data as shown by Fig. 8.

We also examined the quantity $f_2^p/\langle n_p\rangle^2$ calculated for the $\bar{p}n$ and $\bar{p}p$ data which is plotted versus $1/\langle n_p\rangle$ in Fig. 9. This quantity is calculated from the number of charged particle pairs $n_p$ produced in $\bar{p}n$ $[n_p = \frac{1}{2}(n-1)]$ and $\bar{p}p$ $[n_p = \frac{1}{2}(n-2)]$ interactions. In light of the two-component model (pionization and diffraction dissociation) it was shown[17] that $pp$ data obey the relation

$$\frac{f_2^p}{\langle n_p\rangle^2} \simeq \frac{\alpha_d}{\alpha_p} - \frac{|A|}{\langle n_p\rangle} .$$

Here $\alpha_p(\alpha_d)$ is the contribution of the pionization (diffraction dissociation) to the production mechanism, whereas $|A|$ is a parameter depending on $\alpha_p$ and $\alpha_d$.[17] For the $\bar{p}N$ interactions the situation is more complicated because one has to consider the annihilation process in addition to the pionization and diffraction dissociation mechanism. Still neglecting interference phenomena, the $f_2^p$ moment can be expressed as

$$f_2^p = \alpha_\pi f_\pi + \alpha_d f_d + \alpha_a f_a + \alpha_\pi\alpha_d[\langle n_\pi\rangle - \langle n_d\rangle]^2 + \alpha_\pi\alpha_a[\langle n_\pi\rangle - \langle n_a\rangle]^2 + \alpha_a\alpha_d[\langle n_a\rangle - \langle n_d\rangle]^2 ,$$

the $a$, $\pi$, and $d$ indices denoting the annihilation, pionization, and diffraction dissociation contributions to the production mechanism. If one takes the last formula seriously and if one assumes that $\langle n_\pi\rangle \sim \langle n_a\rangle$ and that $\langle n_{\pi,a}\rangle \gg \langle n_d\rangle$ one obtains

$$\frac{f_2^p}{\langle n_p\rangle^2} \simeq B - \frac{|A|}{\langle n_p\rangle} ,$$

$B$ and $A$ now being parameters depending on $\alpha_a$, $\alpha_\pi$, and $\alpha_d$.

Clearly the $\bar{p}N$ data shown in Fig. 9(a) do not obey such a rule. Let us notice, however, that if one plots $f_2^-/\langle n_-\rangle^2$ versus $1/\langle n_-\rangle$, these quantities being calculated from the negatively produced particles, the $\bar{p}N$ data tend to be distributed on a straight line [Fig. 9(b)]. In fact by fitting the $\bar{p}p$ results in the $0.4 < 1/\langle n_-\rangle < 0.7$ range one obtains

$$\frac{f_2^-}{\langle n_-\rangle^2} = (0.17 \pm 0.01) - \frac{(0.82 \pm 0.02)}{\langle n_-\rangle} .$$

Although this result is similar to that found for $pp$ interactions in which $n_p = n_-$ it is rather difficult at this stage to interpret the behavior shown in Fig. 9(b) in terms of production mechanisms. [In any case the form of the above expression is also obtained if one assumes that $c_2 = \langle n^2\rangle/\langle n\rangle^2$ is independent of the incident momentum as then $f_2^-/\langle n_-\rangle^2 = (c_2 - 1) - 1/\langle n_-\rangle$ with $c_2 \simeq 1.25$.[13] (Note that for $\bar{p}n$ interactions an additional term $1/\langle n_-\rangle^2$ will appear.)

## IV. CONCLUSIONS

From the study of $\bar{p}d$ interactions we have determined the $\bar{p}n$ topological cross sections at incident momenta of 5.55, 9.3, and 14.6 GeV/$c$. Despite the uncertainty introduced by analyzing our data with the impulse approximation model we were able to study the incident momentum dependence of the multiplicity distributions. We observed both a broadening of the multiplicity distributions and an increase in the averaged charged multiplicity $\langle n\rangle$ when the incident momentum increases.

By comparing our data with $\bar{p}p$ results we observed the rather remarkable feature that at 14.6 GeV/$c$ the $\bar{p}p$ and $\bar{p}n$ topological cross sections tend to be on a smooth curve. This is different at 5.55 GeV/$c$ where the $\bar{p}p$ and $\bar{p}n$ data present a different behavior. We have also shown that for each of our three incident momenta the dispersion of the charged multiplicity is greater for $\bar{p}n$ than $\bar{p}p$ interactions in contrast to $\langle n\rangle$ which is smaller for $\bar{p}n$ than for $\bar{p}p$. However, the proximity of our $\langle n\rangle$ values to those obtained from $\bar{p}p$ interactions is not compatible with models describing the charged particle production in terms of emission of pairs of oppositely charged particles.

We have also determined that the momenta $c_q = \langle n^q\rangle/\langle n\rangle^q$ $(q = 2, 3, 4)$ calculated from our data are, within the present errors, independent of the incident momentum as expected from the early KNO scaling. In fact our data seem to verify some early scaling behavior although it is different from those presented by $pp$ and $\bar{p}p$ interactions. This may arise from the fact that our $D/\langle n\rangle$ ratio has a value different from those calculated from $\bar{p}p$ and $pp$ interactions. In any case, our number of data points is too small to see if, similarly to $pp$ and $\bar{p}p$ interactions, the dispersion of the $\bar{p}n$ charged multiplicity can be related to its average by a linear relation. Other studies of $\bar{p}n$ interactions

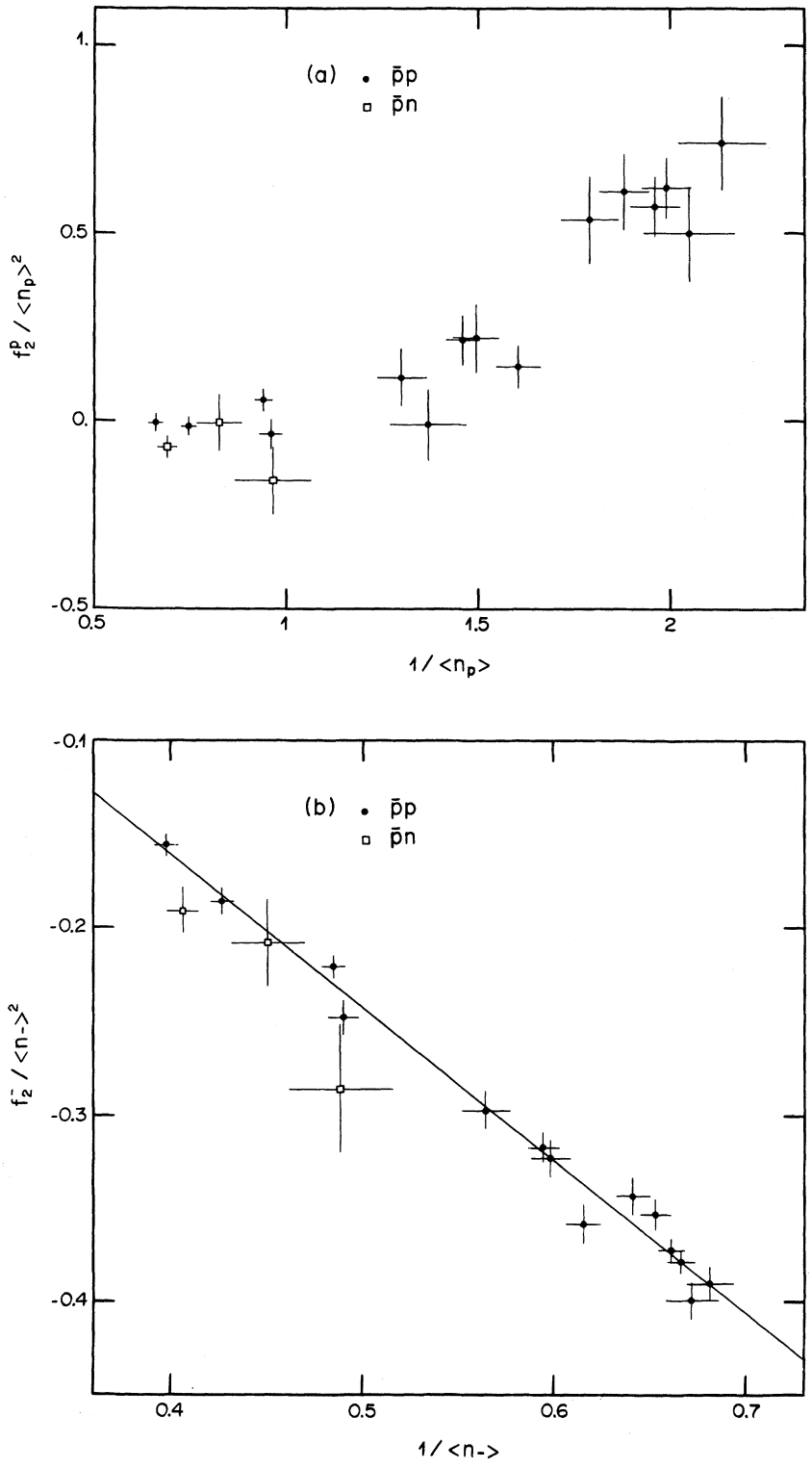


FIG. 9. (a) The $f_2^b/\langle n_b \rangle^2$ ratio plotted versus $1/\langle n_b \rangle$ for the $\bar{p}n$ and $\bar{p}p$ data. These quantities are calculated from the number of charged particle pairs $n_b$ produced in $\bar{p}n$ $[n_b \frac{1}{2}(n-1)]$ and $\bar{p}p$ $[n_b \frac{1}{2}(n-2)]$ interactions. (b) The same distribution calculated this time from the out-going negatively charged particle.

will certainly be useful in order to make a more complete comparison with $\bar{p}p$ and $pp$ interactions. Such a comparison as well as the analysis of new $\bar{p}n$ data is in any case expected to contribute to a better knowledge of multiparticle production phenomena. Furthermore a detailed study of screening and double scattering in the deuteron will certainly be necessary in order to see how these effects will influence the statistical moments studied in this work.

---


[1]In principle, the number of coherent events in the odd-prong events is small because of kinematical suppression. Neverthelsss this number cannot be always neglected. Thus at 5.55 and 14.6 GeV/$c$ the number of events in the $\bar{p}d \to \bar{p}d\pi^+\pi^-$ channel having invisible deuteron recoil is about 20% and 35%, respectively.

[2]A Fridman, Fortschr. Phys. 23, 243 (1975).

[3]D. Evrard, A. Fridman, and A. C. Hirshfeld, Nucl. Phys. B14, 699 (1969).

[4]H. Braun, D. Evrard, A. Fridman, J-P. Gerber, G. Maurer, A. Michalon, B. Schiby, R. Strub, and C. Voltolini, Phys. Rev. D 2, 1212 (1970).

[5]H. Braun, D. Evrard, A. Fridman, J-P. Gerber, A. Givernaud, R. Kahn, G. Maurer, A. Michalon, B. Schiby, R. Strub, and C. Voltolini, Phys. Rev. D 3, 2572 (1971).

[6]The flux-factor correction depends only on the momentum configuration of the incident particle and the bound nucleon. This correction factor, however, can be compensated for by a monotonic decrease of the $\bar{p}n$ cross section in the range of the c.m. energy resulting from the Fermi motion of the neutron target. See for instance Ref. 2.

[7]H. Braun, D. Evrard, A. Fridman, J-P. Gerber, G. Maurer, A. Michalon, B. Schiby, C. Voltolini, and P. Cüer, Phys. Rev. D 2, 488 (1970); H. Braun, A. Fridman, J-P. Gerber, A. Givernaud, P. Juillot, J. A. Malko, G. Maurer, A. Michalon, B. Schiby, and C. Voltolini, *ibid.*, 2311 (1972); H. Braun, D. Brick, A. Fridman, J-P. Gerber, P. Juillot, G. Maurer, A. Michalon, M.-E. Michalon-Mentzer, R. Strub, and C. Voltolini, Phys. Rev. Lett. 33, 312 (1974); H. Braun, D. Evrard, A. Fridman, J-P. Gerber, A. Givernaud, J. Grunhaus, R. Kahn, G. Maurer, A. Michalon, B. Schiby, R. Strub, and C. Voltolini, Z. Phys. 247, 107 (1971).

[8]C. Bracci *et al.*, CERN-HERA Report No. 73-1, 1973 (unpublished).

[9]F. T. Dao, J. Lach, and J. Whitmore, Phys. Lett. 51B, 505 (1974).

[10]H. Braun, D. Brick, A. Fridman, J.-P. Gerber, E. Jegham, P. Juillot, and C. Voltolini, Phys. Rev. D 10, 3573 (1974).

[11]Z. Koba, H. B. Nielsen, and P. Olesen, Nucl. Phys. B40, 317 (1972).

[12]P. Slattery, Phys. Rev. D 7, 2073 (1973).

[13]F. T. Dao, J. Lach, and J. Whitmore, Phys. Lett. 45B, 513 (1973).

[14]E. L. Berger, in Proceedings of the Second International Conference on Elementary Particles, Aix-en-Provence, 1973 [J. Phys. (Paris) Suppl. 34, C1-346 (1973)]. See also A. J. Buras, J. Dias de Deus, and R. Møller, Phys. Lett. 42B, 251 (1973); R. Møller, Nucl. Phys. B74, 145 (1974); P. Slattery, Phys. Rev. D 10, 2304 (1974).

[15]A. Wroblewski, Acta Phys. Pol. B4, 857 (1973).

[16]P. K. Malhotra, Nucl. Phys. 46, 559 (1963).

[17]K. Fiałkowski, Phys. Lett. 41B, 379 (1972).